Nano Energy 105 (2023) 107982

Contents lists available at ScienceDirect

Nano Energy

journal homepage: www.elsevier.com/locate/nanoen

A general self-powered wireless sensing solution based on triboelectric-discharge effect

Haoyu Wang [a], Xin Xia [a,b], Jingjing Fu [a], Jianan Li [c], Chaojie Chen [a], Yuan Dai [c,*], Zhiyong Fan [d], Guobiao Hu [e], Yunlong Zi [a,b,f,g,h,**]

[a] Department of Mechanical and Automation Engineering, The Chinese University of Hong Kong, Shatin, N.T., Hong Kong, China
[b] Thrust of Sustainable Energy and Environment, The Hong Kong University of Science and Technology (Guangzhou), Nansha, Guangzhou, Guangdong 511400, China
[c] Tencent Robotics X, Shenzhen, Guangdong 518054, China
[d] Department of Electronic and Computer Engineering, The Hong Kong University of Science and Technology, Clear Water Bay, Kowloon, Hong Kong, China
[e] Thrust of the Internet of Things, The Hong Kong University of Science and Technology (Guangzhou), Nansha, Guangzhou, Guangdong 511400, China
[f] HKUST Shenzhen-Hong Kong Collaborative Innovation Research Institute, Futian, Shenzhen, Guangdong, China
[g] Department of Mechanical and Aerospace Engineering, The Hong Kong University of Science and Technology, Clear Water Bay, Kowloon, Hong Kong, China
[h] Shenzhen Research Institute, The Chinese University of Hong Kong, Nanshan, Shenzhen, Guangdong 518057, China

ARTICLE INFO

Keywords:
Self-powered system
Wireless sensing
Triboelectric nanogenerator
Triboelectric-discharge effect
Electromagnetic wave
Wireless sensor platform

ABSTRACT

With the rapid growth of the smart city, wireless sensors are highly preferred in plenty of application scenarios. To address the challenges of real-time sensing, power supply, and wireless signal transmission in current wireless sensors, a self-powered wireless sensing e-sticker (SWISE) based on the triboelectric-discharge effect has been proposed. However, the previously designed SWISE can only detect the unquantifiable signal of its own, which limited its applications. Herein, through studies about electromagnetic (EM) wave characteristics, we couple commercial sensors of different mechanics with EM wave generated by the triboelectric-discharge effect to realize a general self-powered wireless sensing solution for various physical signals. In addition, the integrated device is designed to combine with multiple sensors, with the characteristics of being thin and flexible. Based on this solution, a self-powered wireless temperature and pressure sensing system is demonstrated, with an error rate down to 0.18 %, and a multi-point sensing array was also realized for broad potential applications. This work proposes a self-powered wireless sensing platform that is compatible with various commercial sensors with different physical signals, which promises great potential for self-powered wireless sensing in the smart city and Internet of Things, such as robotic dynamic sensing, infrastructure monitoring, human-machine interface, etc.

1. Introduction

With the development of the smart city and Internet of Things, there are high demands for sensor nodes in plenty of application scenarios, such as robotic dynamic sensing, environment monitoring, infrastructure detection, health care, etc [1–6]. Among them, wireless sensing systems are highly preferred [7–11]. Currently, most wireless sensors still need to be powered by wires or batteries [12,13]. However, the wires bring limitations to the sensing system, especially in the harsh environment and dynamic motion systems [14,15]. The batteries suffer from limited lifetime and potential environmental problems, which are difficult to be replaced and applied in some scenarios, such as

Abbreviations: C, capacitance; C_0, system capacitance; C_B, breakdown discharger equivalent capacitance; C_i, TENG equivalent capacitance; C_s, series capacitance in system; C_p, parallel capacitance in system; C_{pa}, parasite capacitance in system; f, frequency; i, current; l, gap distance of the breakdown discharger; L, inductance; L_0, system inductance; L_s, series inductance in system; Q, accumulated charge; Q_0, charges generated by TENG; r, distance between breakdown discharger and receiver; **r**, vector from the origin to the receiver in position (x, y, z); R, resistance; R_0, system resistance; R_s, series resistance in system; R_T, resistance of thermistor; R_p, parallel resistance in system; R_{therm}, resistance of the thermistor at 298.15 K; t, time; T, temperature; T_s, period; U_B, voltage potential on breakdown discharger; U_i, u_i, voltage potential on TENG; V_i, TENG equivalent voltage output; α, adjust constant; τ, decay time; ω_n, natural frequency; ζ, damping ratio.

* Corresponding author.
** Corresponding author at: Thrust of Sustainable Energy and Environment, The Hong Kong University of Science and Technology (Guangzhou), Nansha, Guangzhou, Guangdong 511400, China.
E-mail addresses: jessiedai@tencent.com (Y. Dai), ylzi@ust.hk (Y. Zi).

https://doi.org/10.1016/j.nanoen.2022.107982
Received 7 September 2022; Received in revised form 21 October 2022; Accepted 3 November 2022
Available online 4 November 2022

implantable systems [16–18]. Recently, the emerging nanogenerators which effectively convert tiny mechanical energy to electrical energy may address this problem, serving as the power source for wireless sensing systems [19–24]. However, most of the state-of-art nanogenerator-based wireless sensing systems still require additional components, including a power management circuit and micro control unit, which makes the whole system bulky and complex in structure, showing limitations in broad application scopes [25–28].

To address this issue, our team put forward the concept of tribophotonics as a potential solution to realize the self-powered wireless sensing system via the photons, which can directly convert the input mechanical signal into a wireless signal without complex intermediate steps [29]. In that, as a tribo-induced electromagnetic-wave generation (TIEG) device, the self-powered wireless sensing e-sticker (SWISE) was proposed in our previous work [30]. Based on triboelectric-discharge-induced displacement current, the SWISE can directly convert the input mechanical signal to electromagnetic (EM) wave and thus realize fully self-powered wireless sensing, achieving the longest effective transmission distance with the smallest system size among current wireless sensing systems. However, the previously designed SWISE can only realize the functions of motion sensing and gas sensing, while it is still difficult to be used for wireless sensing of multiple other kinds of physical signals. Considering the potential application towards various kinds of sensing scenarios, such as infrastructure detection, human healthcare, and environment monitoring, it is still expected to realize a general solution to achieve self-powered wireless sensing for varieties of physical, chemical, and biomedical signals.

Here, we coupled the EM-wave signal generation and commercial sensors to realize a general triboelectric-discharge effect enabled self-powered wireless sensing solution (TDE-SWIS) for various physical signals. Considering the influence given by different parameters in the TDE-SWIS, we proposed the equivalent circuit model and simulated the EM-wave characteristics, which were consistent with the experimental results. Then, a self-powered wireless sensing platform coupling with resistive, capacitive, and inductive sensors was achieved, targeting different practical applications. The integrated TDE-SWIS device was further designed to combine with multiple sensors to realize self-powered wireless sensing with thin and flexible characteristics. The self-powered wireless temperature sensing system and self-powered wireless pressure sensing system were demonstrated. Furthermore, such a modulation strategy can also be applied for distinguishing different TDE-SWIS signals to realize multi-point sensing. Thus, based on the characteristics of real-time, self-powered, wireless, and the function of sensing platform, this approach is suitable for most commercial sensors and shows great potential for many application scenarios of smart city, such as infrastructure monitoring, environment monitoring, industrial sensing, etc.

2. Main text

2.1. Theoretical model of TDE-SWIS

The concept of TDE-SWIS is illustrated in Fig. 1a. The commercial sensors, depending on sensing mechanisms of variations in resistance, capacitance, or inductance, were coupled in the equivalent circuit for the triboelectric-discharge unit (TDU), including a TENG part (the TENG part in Fig. 1a is shown separately from TDU to highlight the mechanical energy input) and a breakdown discharger (BD) (shown in Fig. S1), as shown in Fig. 1b-I. Here, the TENG was equivalent to a voltage source connected with a variable capacitance C_i in series. The R_0 and L_0 presented the system resistance and inductance, respectively. When there was a mechanical signal input, the charges were accumulated on the TENG and BD, as shown in Fig. 1b-II, where the BD can also be considered as a capacitor C_B. Here, the charges on TENG and BD were Q_i and Q_B, respectively. Once the voltage potential U_B on the BD is higher than the breakdown threshold voltage given by Paschen's law, the breakdown discharge effect happened. In this process, the avalanche and plasma were generated across the gap of the BD, as shown in Fig. 1b-III. The induced current i oscillated with high frequency, given by Fig. 1c, can generate the EM wave signal, which can be detected by a receiver in the distance. And then, the wireless signals were generated and transmitted, where the received electric field intensity was mainly related to the i and $\frac{di}{dt}$[31]. The details and derivations were discussed in Note S1 and S2. After the signals were received by an antenna and went through the signal processing, the target physical signals, such as temperature, pressure, humidity, etc., can be resolved through key parameters in the signals.

The oscillation in the wireless signals generated from the system can be calculated by the equivalent circuit as shown in Fig. 1b-III, which can

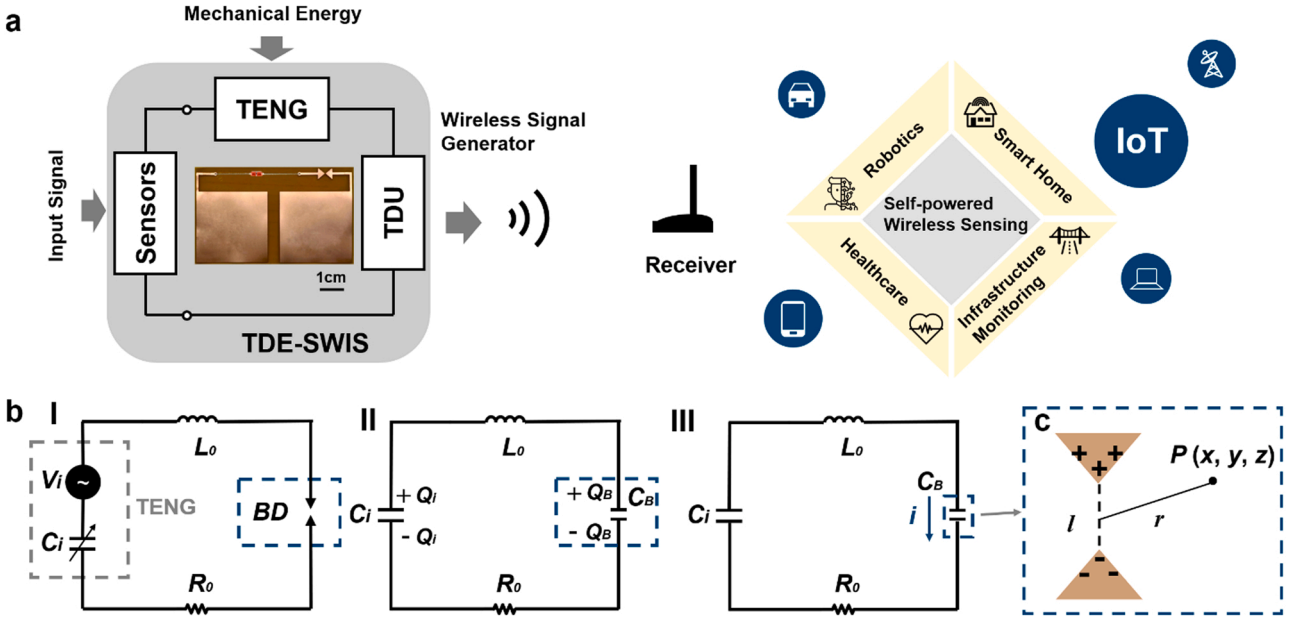

Fig. 1. The overall illustration of triboelectric-discharge effect enabled self-powered wireless sensing platform and theoretical model. (a) The schematic illustration of the working process of TDE-SWIS. (b) The equivalent circuit in (I) initial status, (II) charged status, and (III) discharge status. (c) The EM model of BD.

be considered as a resistor-inductor-capacitor (RLC) circuit, where the equivalent resistor, inductor, and capacitor were noted to R, L, C respectively. The current in the system is reflected by Kirchhoff's voltage law:

$$L\frac{di}{dt}+Ri+\frac{1}{C}\int idt=u_i(t) \tag{1}$$

where $u_i(t)$ presents the voltage potential on TENG. Compared with the period of the breakdown process, the period of the input mechanical signal was much longer. Thus, once the voltage of the BD approached the threshold voltage, the voltage decreased to zero instantaneously, which is equivalent to the conducting status. Thus, the input voltage $u_i(t)$ can be considered as a step function, and the step current response can be solved in three different damping conditions with the detailed solving process shown in Note S3. Here, the parameters were adjusted to natural frequency $\omega_n=\sqrt{\frac{1}{LC}}$ and damping ratio $\zeta=\frac{R}{2\sqrt{\frac{L}{C}}}$.

The three damping conditions include:

1) Underdamping condition: when $0\le\zeta<1$, the current response can be solved as:

$$i(t)=\frac{1}{L\omega_n\sqrt{1-\zeta^2}}e^{-\zeta\omega_n t}\sin\left(\omega_n\sqrt{1-\zeta^2}\,t\right) \tag{2}$$

2) Critical-damping condition: when $\zeta=1$, the current response can be solved as:

$$i(t)=\frac{1}{L}te^{-\omega_n t} \tag{3}$$

3) Over-damping condition: when $\zeta>1$, the current response can be solved as:

$$i(t)=\frac{1}{2L\omega_n\sqrt{\zeta^2-1}}\left[e^{\omega_n\left(-\zeta+\sqrt{\zeta^2-1}\right)t}-e^{\omega_n\left(-\zeta-\sqrt{\zeta^2-1}\right)t}\right] \tag{4}$$

By applying the inductor-capacitor-resistor (LCR) meter, the system capacitance C_0 was around 5.713 pF, and the system inductance L_0 was

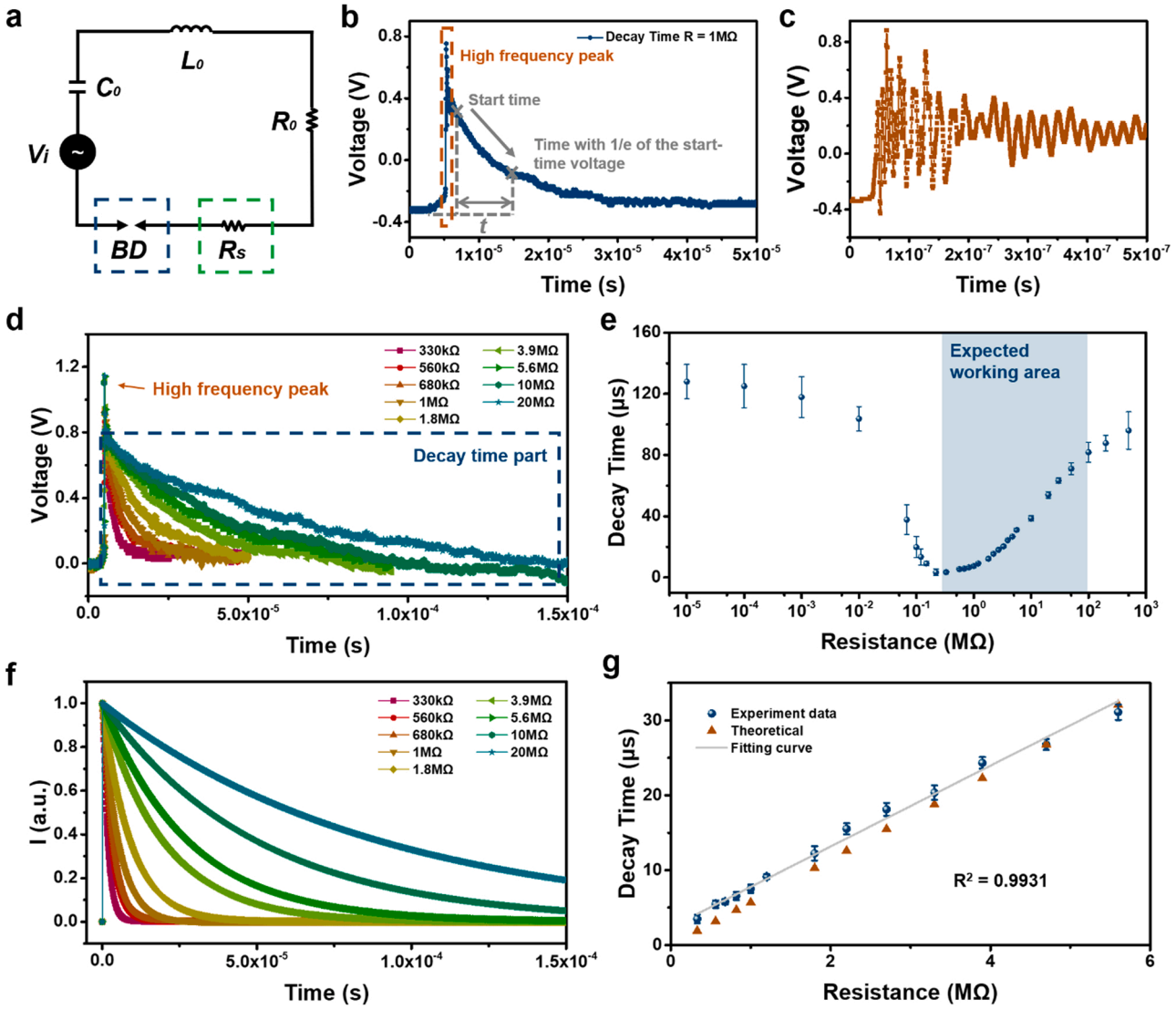

Fig. 2. Resistance-based TDE-SWIS signal coupling. (a) The equivalent circuit of the resistance-based TDE-SWIS signal coupling towards damping ratio. (b) The demonstration of medium-frequency decay signal and the calculation method of the decay time. (c) The high-frequency pulse signal of TDE-SWIS. (d) The time-domain medium-frequency decay signal of TDE-SWIS towards different R_s. (e) The relationship between the decay time and R_s, which can be divided into three regions. (f) The theoretical result of normalized time-domain TDE-SWIS signal of different R_s. (g) The comparison of experiment result, theoretical result, and fitting curve of the decay time and R_s.

around 2.713 μH, as recorded from the system in our experiments. Substituting these parameters to Eqs. 2–4 and adjusting the ζ, the corresponding waveforms were shown in Fig. S2. Based on this principle, the parameter of ζ and ω_n of the wireless signal can be adjusted, by the resistance, inductance, and capacitance values in the system. Compared with the high-frequency SWISE signal due to the discharge process, this oscillation-induced signal in 5 kHz-5 MHz was much easier to be detected and processed, with the much lower requirement of the receiver system. Thus, the modulations of the wireless signal from TDE-SWIS can be realized through parameter (resistance, inductance, capacitance) variations brought by sensors.

2.2. Resistance-based TDE-SWIS signal coupling method

Firstly, as the ζ can be adjusted by the resistance, an external resistor R_s was coupled into the TDE-SWIS system in series to tune the output EM signal, as shown in Fig. 2a. The TDE-SWIS system mainly consisted of a free-standing mode TENG (FS-TENG) and a BD, and the external resistor was serially connected by wires. By using an LCR meter, the system capacitance C_0 (including the capacitance from the TENG and wires) was around 5.713 pF, and the system inductance L_0 was around 2.713 μH. The resistance from the system was too small and could be ignored, as compared with the external resistor. With the transmission distance of 1 m, a monopole antenna with a length of 30 cm connecting with an oscilloscope was applied to capture and measure the EM signal wirelessly.

As fixed in the optical platform, the FS-TENG was driven by a well-controlled linear motor to ensure a stable mechanical input. With the mechanical signal input, a typical time-domain EM signal coupling the external resistor R_s was shown in Fig. 2b, with the R_s of 1 MΩ. The signal consisted of the high-frequency pulse signal due to the discharge process (around 30 MHz–300 MHz) and the medium-frequency signal due to the electrical oscillation in the circuit (around 5 kHz–5 MHz). The high-frequency pulse signal, as highlighted by the dark orange block, was comprehensively discussed and studied in our previous study [30], where the detailed waveform was shown in Fig. 2c.

By adjusting the external resistance, the decay time of the medium-frequency signal (shown in Fig. 2b) can be manipulated to involve the resistance information. In engineering, the decay time τ is defined as the elapsed time required for the system response to decay in the value of 1/e. The wireless signal can be considered as the combination of the high-frequency pulse signal with large amplitude and medium-frequency decay signal. To avoid the influence of the high-frequency signal on the calculation of the signal decay time, the time of 1.25 μs after the high-frequency peak signal was chosen as the start time of τ, as shown in Fig. 2b. The biasing voltage from the instrument and environment was also considered in the calculation of decay time. Thus, the decay time is the relative value instead of absolute value, which is more meaningful. With the resistance from ~Ω scale to ~GΩ scale, the measured decay time was shown in Fig. 2d. The signal decay trend changed with different series resistance, and the relationship between the decay time and R_s was concluded in Fig. 2e. Considering the practical applications to transmit target sensing signal, the decay time can be divided into three regions.

The first region was with the resistance from 1 Ω to around 220 kΩ. The decay time in the first region gradually decreased from a high value (around 130 μs) to a low value (around 6 μs) with large error bars. The third region was with the resistance from 100 MΩ to GΩ scale. In this region, the decay time increased slowly with the increase of the resistance, gradually approaching a limit with big error bars. Thus, both the first and third regions were difficult to be applied for wireless transmission. The second region was with a resistance from around 220 kΩ to around 100 MΩ, where some of the corresponding waveforms were shown in Fig. 2d. The decay time in the second region monotonically increased with low error bars. Thus, it is suitable for transmitting the signal through TDE-SWIS system, as defined as the expected-working-range region. With $\zeta > 1$ in over-damping condition, the current response can be calculated by Eq. 4, where the normalized theoretical results corresponding to resistance were shown in Fig. 2f, which was generally consistent with experimental results from Fig. 2d without considering the high-frequency peaks, as encircled by dashed lines. Thus, considering the expected working area (220 kΩ to 6 MΩ) only, based on the RLC model, a linear function was applied to describe the relationship between the decay time τ and external resistance R_s, as shown below:

$$\tau = R_s C_0 + \alpha \tag{5}$$

where α is the adjustment constant. The fitting curve, experiment data and theoretical result were shown in Fig. 2g, where the experimental results matched the theoretical results. Thus, this region can be widely applied for TDE-SWIS wireless sensing based on resistance variation.

2.3. Capacitance and inductance-based TDE-SWIS signal coupling method

Based on the definition of damping ratio, ζ can also be adjusted by capacitance. The influence of series capacitance C_s was tested, and the equivalent test circuit was shown in Fig. 3a, where C_s was highlighted by the green box (Fig. 3a-I). Similarly, the received TDE-SWIS signal was analyzed by decay time, and the relationship between the decay time and C_s was shown in Fig. S3a. It was kept in high value when C_s was lower than around 30 pF, and gradually decreased from 30 pF to 300 pF. Besides the R and C_s, the series inductance L_s can also adjust ζ in TDE-SWIS system. The experiment circuit was set as replacing the series capacitance C_s by a series inductance L_s in the highlighted green box, as given in Fig. 3a-II. With the increase of L_s, the decay time was shown in Fig. S3b. The decay time was almost kept in a constant value with the increase of the inductance, which satisfied the theory result, as shown in Fig. S3c, where the difference in measured result may be due to the impact of resistance in inductors.

Besides ζ, ω_n can also be manipulated to modulate the TDE-SWIS signal. The L_s can make an influence on the ω_n, and the base frequency of each TDE-SWIS signal gradually decreased with the increasing L_s, where the base frequency can be calculated by the equation below:

$$f = \frac{1}{2\pi\sqrt{(L_s + L_0)C_0}} \tag{6}$$

Here, the corresponding time-domain signal was shown in Fig. S4, in which is consistent with our previous study [30].

Alternatively, by combining the inductors and capacitors in TDE-SWIS circuit, the capacitor can also be applied to adjust ω_n. By connecting C_s with L_s in series, C_s can be applied to modulate ω_n, as given by Fig. 3a-III. Thus, the base frequency can be adjusted by:

$$f = \frac{1}{2\pi\sqrt{(L_s + L_0)\left(\frac{C_0 C_s}{C_0 + C_s}\right)}} \tag{7}$$

Here, the time-domain signal was shown in Fig. S5a. In addition, the base frequency in the time domain can also be converted to the period T_s as illustrated by:

$$T_s = \frac{1}{f} \tag{8}$$

The comparison between the experiment result and the theory was shown in Fig. S6.

By connecting the C_p with L_s in parallel, the ω_n can also be modulated, as given by Fig. 3a-IV. In this case, the base frequency can be adjusted to:

$$f = \frac{1}{2\pi\sqrt{(L_s + L_0)(C_0 + C_p)}} \tag{9}$$

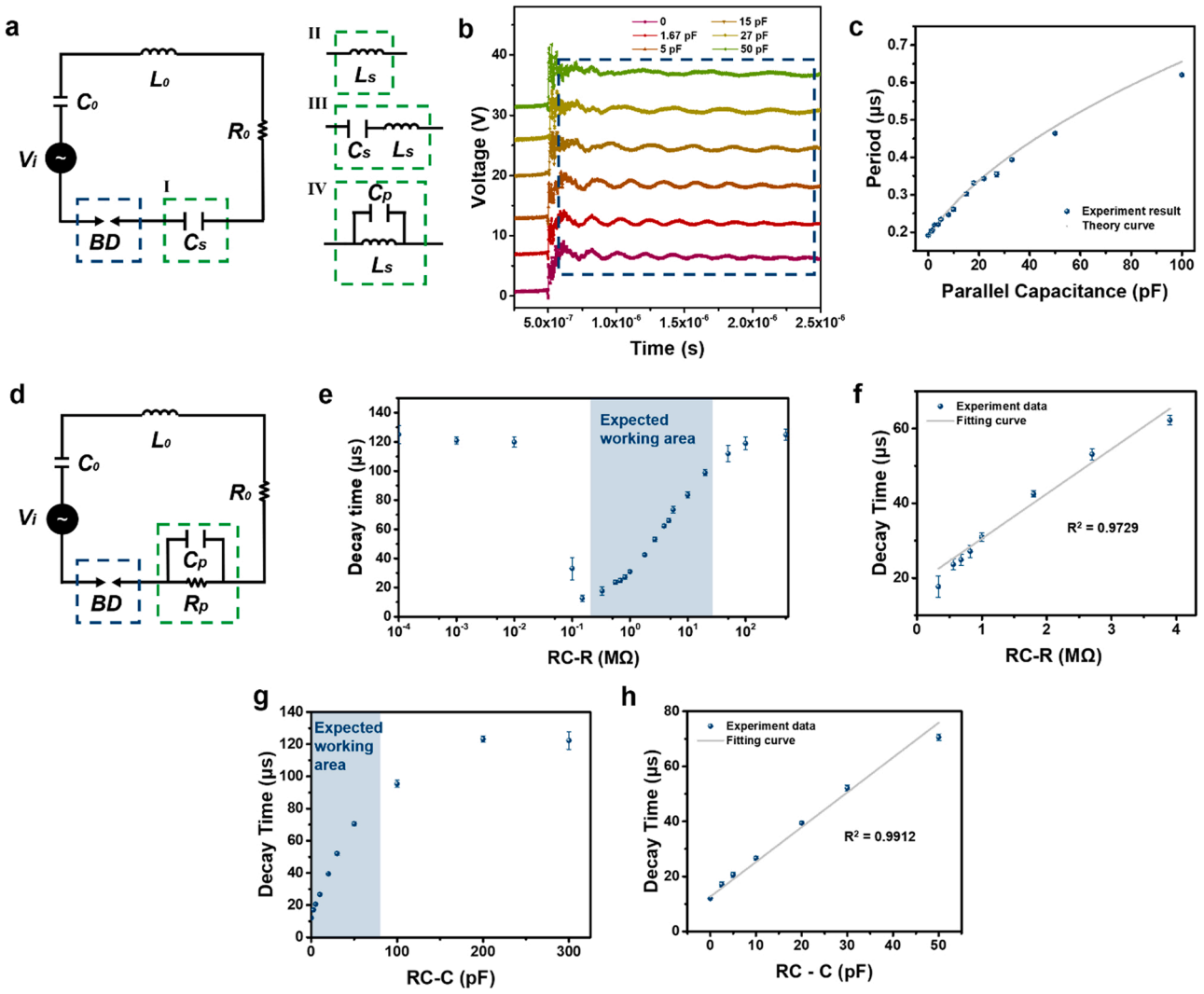

Fig. 3. Capacitance and inductance-based TDE-SWIS signal coupling and the parallel resistance and capacitance-based TDE-SWIS signal coupling. (a) The equivalent circuit of the (I) C_s (II) L_s-based signal coupling towards damping ratio and the (III) C_s connected with L_s (IV) C_p connected with L_s-based signal coupling modulation methods towards natural frequency. (b) The selective time domain TDE-SWIS signals in different parallel capacitance in signal coupling towards ω_n (c) The relationship between the period and parallel capacitance C_p. (d) The equivalent circuit of the *RC* parallel model-based TDE-SWIS signal coupling. (e) The relationship between the decay time and series resistance in the *RC* parallel model. (f) The decay time had an almost linear relationship with the series resistance with the range around 220 kΩ to 4 MΩ in *RC* model. (g) The relationship between the decay time and parallel capacitance in *RC* parallel model. (h) The decay time had an almost linear relationship with the parallel capacitance with the range around 0–50 pF in the *RC* parallel model.

By applying a different value of C_p, the time domain waveforms were shown in Fig. 3b, where the base frequency oscillation signal was also highlighted by the dark blue block. The detailed waveforms were further shown in Fig. S5b. As shown by the time domain waveforms, with the increasing parallel capacitance, the period of the oscillation increased and the amplitude of that decreased. By collecting the corresponding data, the comparation between the experiment result and theoretical curve was shown in Fig. 3c. The experiment result was fitted with the Eq. 9 with small error bars, which can be applied for the wireless signal transmission of the capacitance.

2.4. Parallel resistance and capacitance-based TDE-SWIS signal coupling method

In practical applications, capacitive and resistive sensors usually cannot be directly considered as pure capacitors or resistors, respectively. For example, a thin-film capacitive pressure sensor involves a low capacitance (pF scale) with high resistance (GΩ scale). Then the equivalent circuit of it was considered as a large resistor connected with a small capacitor in parallel. Thus, to deal with these problems in practical applications, the *RC* parallel model was studied, as shown in Fig. 3d, where a resistor and capacitor were connected in parallel with each other and connected to the TDE-SWIS system in series.

Firstly, when C_p was fixed to 10 pF with a gradually increased resistance value, the decay time was shown in Fig. 3e. Similar to the case in Fig. 2e, the curve can also be divided into three regions. The fitting curve and the experiment data in expected-working-range were shown in Fig. 3f, demonstrating the high linearity. Thus, towards a more universal application scenario, the theory of *R*-based TDE-SWIS signal coupling can be adjusted to:

$$\tau = R\left(C_0 + C_p + C_{pa}\right) + \alpha \tag{10}$$

where the C_p and C_{pa} present parallel capacitance and parasite capacitance, respectively. Here, the parasite capacitance was generated when the TDE-SWIS system was placed near conductors, which has to be considered in practical applications.

Secondly, when the R_p was fixed to 1 MΩ with gradually increasing C_p, the decay time was shown in Fig. 3g. With the increasing

capacitance, the decay time monotonically increased with small error bars. Thus, the signal was much easier to be distinguished, especially in the low capacitance situation. The decay time increased in a linear relationship with the capacitance with small errors for the parallel capacitance lower than around 75 pF, which was defined as the expected-working-area. When the parallel capacitance was larger than 75 pF, the decay time approached the limit with larger error bars, which may not be used for wireless sensing.

2.5. Influences from environmental factors on TDE-SWIS signals

In the previous study [30], we noted both the output signals of TENG and TDE-SWIS could be influenced by the environmental factors, especially the humidity and temperature. Here, an experiment platform was built to analyze the influence of humidity and temperature on TDE-SWIS signals. Firstly, the BD was placed into a temperature box, and the FS-TENG was placed outside, where the temperature box was sealed, and the temperature could be controlled, as shown in Fig. S7a. With the increasing temperature, there was little influence on the TDE-SWIS signal in the frequency domain, as shown in Fig. S7b. Secondly, the BD was placed into a sealed acrylic box and driven by an FS-TENG outside of the box, where the humidity inside the box can be controlled. The TDE-SWIS signal under different humidity in the frequency domain was shown in Fig. S8. With the increasing humidity, the frequency and amplitude of the TDE-SWIS signal changed. Especially for the high humidity part (> 85 %), the amplitude in the high-frequency region (> 150 MHz) gradually decreased to zero. In general, the TDE-SWIS signal was barely dependent on environmental temperature but dependent on the humidity in some extent.

2.6. TDE-SWIS-based self-powered wireless temperature sensing system

With the characteristic of fully self-powered wireless sensing, the TDE-SWIS can be applied to wireless sensing platform by coupling different kinds of commercial sensors towards different application scenarios, without any additional power source or wire needed. As reported by our previous study [30], the TDE-SWIS is able to deliver a long effective transmission distance (up to 30 m), which satisfied the demands of sensing networks of smart city. To demonstrate the effective signal wireless transmission ability of the sensing platform, we designed two applications of the TDE-SWIS-based self-powered wireless sensing by involving commercial resistive and capacitive sensors, respectively, which are considered as two major types of sensors in the market.

We combined the commercial resistive temperature sensor (thermistor, MF58 1M4400) with TDE-SWIS system to realize self-powered wireless temperature sensing. Here, the system circuit consisted of the

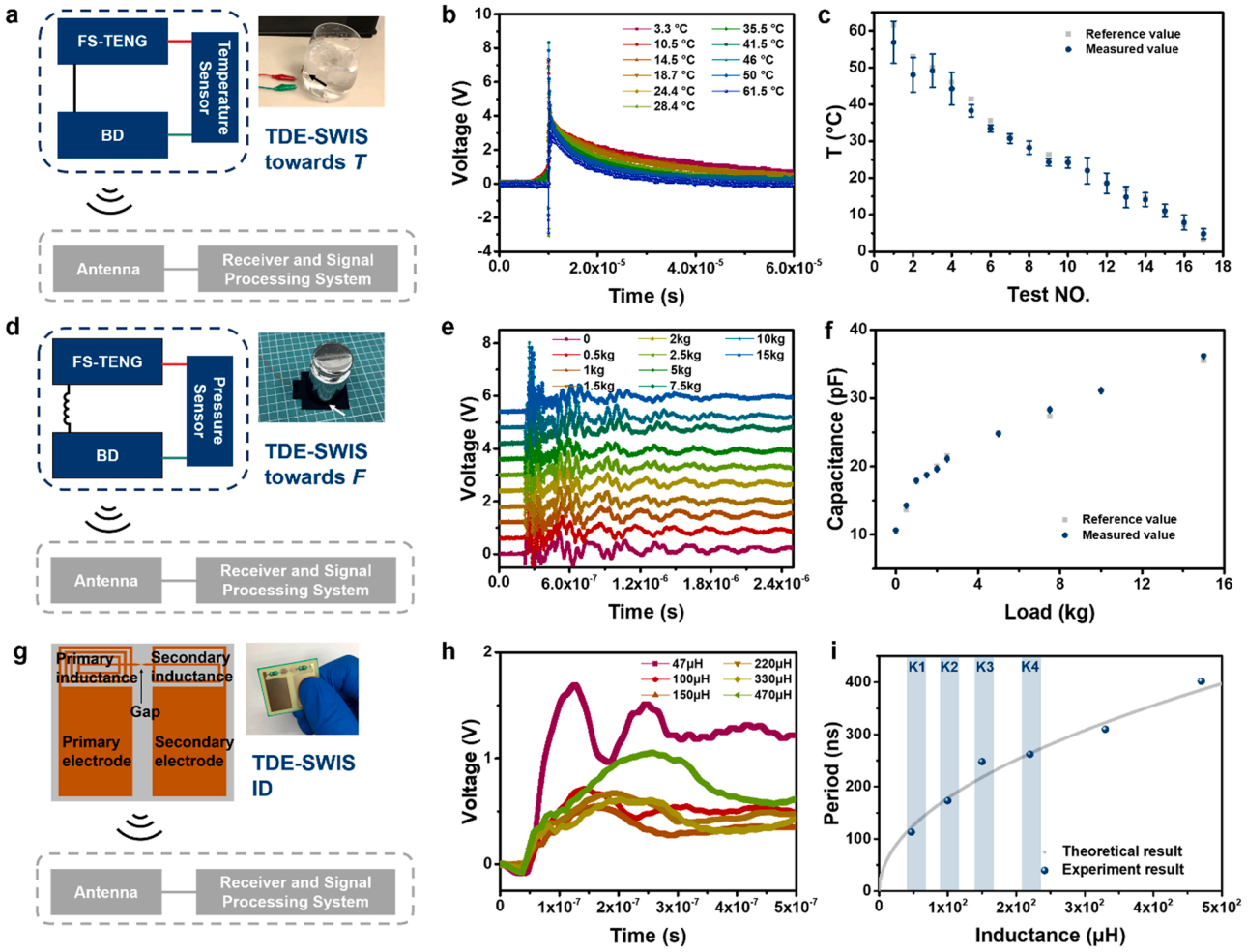

Fig. 4. The TDE-SWIS-based self-powered wireless sensing systems and multi-points sensing device. (a) The TDE-SWIS-based self-powered wireless temperature sensing system towards glass cup wall temperature monitoring. (b) The time domain TDE-SWIS signal under different temperature. (c) The comparation of reference value of temperature with TDE-SWIS tested result. (d) The TDE-SWIS-based self-powered wireless pressure sensing system. (e) The time-domain TDE-SWIS signal under different load pressure. (f) The comparation of reference value of load pressure with TDE-SWIS tested result. (g) The designed multi-point sensing TDE-SWIS device based on inductance-based TDE-SWIS signal coupling. (h) The time domain signal of TDE-SWIS device with different series inductance. (i) The comparison of the period of TDE-SWIS devices with the theoretical curve.

FS-TENG, BD, small adjusted resistor, and temperature sensor connected in series. An antenna was applied to collect the transmitted EM wave signals with the distance of 1 m, which can be further processed by the oscilloscope and computer to directly illustrate the measured temperature. Here, the resistance of the chosen commercial temperature sensor R_T changed with the temperature, given by the equation below:

$$R_T = R_{therm} e^{4400\left(\frac{1}{T}-\frac{1}{298.15}\right)} \tag{11}$$

which was within the expected working area, as stated in Fig. 2e, where R_{therm} presents the resistance of the temperature sensor at 298.15 K. Thus, the resistance of the temperature sensor can be transmitted by the system in a self-powered wireless manner. Here, the temperature sensor was attached to a glass cup wall to monitor the cup wall temperature, as shown in Fig. 4a, where the thermal grease and thermal insulation foam tape were applied to make sure the constant temperature condition of the temperature sensor. A multichannel temperature testing equipment (anbai AT4716) was applied to monitor the temperature of the cup wall as the standard value, where the probe was also attached to the cup wall. Here, we applied hand motion to simulate the input mechanical energy. With the hand motion, the time-domain TDE-SWIS signals under different glass cup wall temperatures were detected wireless, as shown in Fig. 4b, where the decay time increased with the decreasing of cup wall temperature. Based on Eq. 10 and Eq. 11, the wireless signal can be further processed, and the measured temperature was illustrated by computer via Python, where the collected data can be transmitted from the oscilloscope to computer via USB interface. The detailed data processing process was discussed in Materials and methods part. Here, several groups of cup wall temperature cases with the range from 3.3 ℃ to 61.5 ℃ were tested, and the comparison between the measured result (gray dot) and TDE-SWIS transmitted result (dark blue dot) was shown in Fig. 4c. The working process of the self-powered wireless temperature sensing system was shown in Fig. S9 and Video S1. The performance of the temperature sensing system can be further improved by applying a more suitable commercial resistive sensor and adjusting the commercial resistive sensor to a more suitable working range. Thus, the demonstrated system can be applied for self-powered wireless temperature sensing, especially the scenarios such as implantable system temperature sensing, environment monitoring, infrastructure monitoring, etc. In addition, the TDE-SWIS system can be applied for the application of signal transmission towards multiple commercial resistive sensors in different application scenarios towards different target signals.

Supplementary material related to this article can be found online at doi:10.1016/j.nanoen.2022.107982.

2.7. TDE-SWIS-based self-powered wireless pressure force sensing system

The commercial capacitive pressure sensor was combined with the TDE-SWIS system to realize self-powered wireless pressure sensing. The signal of the capacitive sensor can be transmitted by the *RC*-based TDE-SWIS signal coupling (given by the relationship between decay time and capacitance, as shown in Fig. 3h) or *LC*-based TDE-SWIS signal coupling (given by the relationship between period and parallel capacitance, as shown in Fig. 3c) via TDE-SWIS system. Here, we mainly demonstrated the *LC*-based TDE-SWIS signal coupling to transmit the signal of capacitive sensors. The capacitive pressure sensor was connected to the inductor with an inductance of 100 μH in series to be involved in TDE-SWIS circuit, as shown in Fig. 4d. Here, the pressure was controlled by the different weights. Similarly, when there was a hand motion input in the TENG part, the TDE-SWIS signals were generated and detected wirelessly, as shown in Fig. 4e. The detected signals were further processed by the median filter to calculate the capacitance of the pressure sensor. The system capacitance C_0 can be calculated by the detected TDE-SWIS signal without connecting capacitive pressure sensors. The detailed data processing process was discussed in Materials and methods part. Additionally, the capacitance of the pressure sensor under different loads was measured by the LCR meter as the standard value. The comparison between the reference value and the TDE-SWIS transmitted capacitance was shown in Fig. 4f with the low error rate of down to 0.18 %. The result showed high accuracy and thus can transmit the capacitance value of the pressure sensor effectively. In addition, an integrated TDE-SWIS device was designed, which can be directly integrated with the commercial sensors to transmit the sensing signal with the characteristics of thin (with a thickness of 43 μm) and flexible, as shown in Fig. S10. The integrated TDE-SWIS device-based demonstration was shown in Fig. S11 and Video S2. Thus, by combining with TDE-SWIS system, the data from capacitive sensors, including but not limited to pressure sensors, can be transmitted in a self-powered wireless style effectively.

Supplementary material related to this article can be found online at doi:10.1016/j.nanoen.2022.107982.

2.8. Integrated TDE-SWIS multi-point sensing system

Except wireless sensing for individual signals, the TDE-SWIS can also be applied to distinguish signals from different sensors to realize multi-point sensing. To demonstrate the multi-point wireless sensing ability, we integrated the inductors with the small-sized TDE-SWIS devices, as shown in Fig. 4g. The integrated system consisted of the primary electrode and secondary electrode to collect induced charge from triboelectricity, primary inductance and secondary inductance to tune inductance, and gap structure for discharge. The printed circuit board (PCB)-based TDE-SWIS device with the size of 3 cm × 3 cm and color ring inductors were firstly applied to verify the effectiveness of our design, which can be further improved by the micro-electromechanical systems (MEMS) technology to realize the thin, flexible, and minimized device. When applying an input force to slide through the device, the wireless signal was detected by the receiver wirelessly, where the received signals with different integrated inductance were shown in Fig. 4h. The comparison between the experiment result and theoretical curve was shown in Fig. 4i, where the experiment result was consistent with the theoretical one. Thus, by applying the different inductors, the wireless signal from different devices can be distinguished. Based on this, the TDE-SWIS array of 2 × 2 can be realized, where the frequency discrimination range of different keys was shown in Fig. 4i. The array was designed in Figs. S12 and S13, and the working process was shown in Video S3. Here, to focus on the whole working process, the data transmission and processing time was shortened in the demonstrated videos.

Supplementary material related to this article can be found online at doi:10.1016/j.nanoen.2022.107982.

3. Conclusion

This work studied the EM and electrical characteristics of the TDE-SWIS system and thus demonstrated it as a general self-powered wireless sensing solution. By adjusting the system parameters such as resistance, inductance, and capacitance, the natural frequency and damping ratio are modulated, which can be characterized by the oscillation base frequency/period and decay time in wireless signals, respectively. The TDE-SWIS signal modulation can be achieved through the *R*-based, *C* and *L*-based, *RC*-based, and *LC*-based coupling methods. Based on these methods, the TDE-SWIS can couple resistive, capacitive, and inductive commercial sensors to transmit the sensed signal of multiple physical signals via EM wave in real-time, self-powered, and wireless manners. The self-powered wireless temperature and pressure sensing systems were demonstrated with different modulation methods. Besides, the integrated thin and flexible TDE-SWIS device was designed for different application scenarios, and the error rate can be down to 0.18 %. The multi-points sensing integrated device was also designed, which showed great potential to realize integrated and minimized wireless sensing

platforms in the future. To conclude, the TDE-SWIS-based self-powered sensing platform demonstrates the advantages of fully self-powered, wireless, real-time, long-distance, and high sensitivity, which is generally applicable for multiple sensors with great potential towards varieties of sensing application scenarios in smart city.

4. Materials and methods

4.1. Fabrication and characterization of FS-TENG

The FS-TENG consisted of the moving part and stationary part. The moving part was fabricated to a nitrile butadiene rubber (NBR) block with the size of 95 mm by 146 mm by 25 mm. The NBR block was made by an NBR film attached to the acrylic and foamed plastic, working as the positive material. The stationary part consisted of the acrylic substrate, electrodes, and fluorinated ethylene propylene (FEP) film. Two copper electrodes with the size of 95 mm by 150 mm were attached to the acrylic plate with the size of 200 mm by 150 mm, working as the electrodes, where two wires were connected to the electrodes separately. Then, an FEP film was attached to the acrylic plate and electrodes layer, working as the negative material. Thus, when there was a relative movement between the moving part and the stationary part, based on the working principle of triboelectrification and electrostatic induction, the high-voltage and low-current outputs were generated on the electrodes. The transferred charges and the output voltage can be measured by the electrometers (Keithley 6514). Here, given by the limitation of the maximum voltage measurement range of the Keithley 6514, the Keithley 6514 was working as a current meter series connected with a high resistance (in GΩ scale). Then, the output voltage of FS-TENG can be calculated by Ohm's law.

4.2. The receiver system

To avoid the influence generated by the LC resonant in the receiver system, a monopole antenna was applied to receive the EM wave generated by the triboelectric-discharge effect. The antenna was connected with the oscilloscopes to collect the signal. Here, many oscilloscopes were applied to verify and collect the signals, including the Keysight DSOX2014A, Tektronix TBS 1102, Tektronix MSO56, and Rigol DS1104Z. The oscilloscope was set in pulse trigger mode or edge trigger mode when collecting the data.

4.3. The data processing of the TDE-SWIS-based self-powered wireless temperature sensing system

The data processing mainly consisted of 5 steps. In this demonstration, we mainly applied the Rigol DS1104Z to collect the EM wave signal data. Firstly, the data collected by the oscilloscopes was transferred to the computer via the universal serial bus test and measurement class (USB-TMC) interfaces. Secondly, the signal pre-processing was applied to the transferred data, where the median filter was applied to the signal to avoid the influence of the noise. Thirdly, the decay time of the signal was calculated. In details, the base value was calculated by the average voltage value before the trigger time point of EM signal and the maximum value was given by the average voltage value near the time of 1.25 μs after the high-frequency peak signal. The corresponding voltage of the decay time point can be calculated based on the base value and maximum value. Then, the average decay time can be calculated by finding the points with the closest distance to the decay time corresponding voltage value in the received TDE-SWIS signal. Thus, the decay time of the signal was calculated. Fourthly, the corresponding resistance of the sensing system can be calculated based on the relationship between the decay time and resistance, as given by Eq. 10 in the main text. Finally, by calculating the corresponding sensor value and decoupling the corresponding measured physical signal, the target physical signal can be solved. In details, the resistance of the temperature sensor can be further calculated by the calculated resistance value of the sensing system. Then, the temperature value can be calculated by the formula which gives the relationship between the resistance and the temperature, as given by Eq. 11 in the main text. Thus, the temperature value can be calculated. The whole data processing process was realized by the Python in PyCharm. The received EM wave signal and the final results were further demonstrated by the GUI interfaces.

4.4. The data processing of the TDE-SWIS-based self-powered wireless pressure sensing system

Before the data processing of the TDE-SWIS-based self-powered wireless pressure sensing signal, the pre-calibration was needed. In this demonstration, we mainly applied the Rigol DS1104Z to collect the EM wave signal data. In the pre-calibration process, the capacitive pressure sensor was not connected to the TDE-SWIS system. Firstly, the data collected by the oscilloscopes was transferred to the computer via the USB-TMC interfaces. Secondly, the signal pre-processing was applied to the transferred data, where the median filter was applied to the signal to avoid the influence of the noise. Thirdly, the time of each extreme point (including the maximum point and minimum point) was calculated. Thus, the period can be calculated by the average value of each difference of corresponding extreme point group. Finally, the system capacitance can be calculated. Here, compared with the system capacitance, the inductance mainly came from the external series-connected inductor, which was much easier to determine. Then, based the Eq. 6, the system capacitance can be calculated. After the pre-calibration, the capacitive pressure sensor was connected to the TDE-SWIS system. After receiving the TDE-SWIS signal in the receiver system, with the same signal processing methods, including the data collection, signal pre-processing, and base period calculation, the overall capacitance can be calculated by Eq. 9. Then, the capacitance of the pressure sensor can be calculated, where the system capacitance has been calculated in the pre-calibration process. Finally, compared with the data sheet of the pressure sensor, the pressure value was shown. The whole data processing process was realized by the Python in PyCharm. The received EM wave signal and the final results were further demonstrated by the GUI interfaces.

CRediT authorship contribution statement

Haoyu Wang: Conceptualization, Methodology, Software, Validation, Formal analysis, Investigation, Data curation, Writing – original draft, Writing – review & editing, Visualization, Project administration. **Xin Xia:** Investigation, Data curation, Writing – review & editing. **Jingjing Fu:** Investigation, Data curation. **Jianan Li:** Software. **Chaojie Chen:** Investigation. **Yuan Dai:** Conceptualization, Methodology, Formal analysis, Resources, Writing – review & editing, Supervision. **Zhiyong Fan:** Writing – review & editing. **Guobiao Hu:** Writing – review & editing. **Yunlong Zi:** Conceptualization, Methodology, Formal analysis, Resources, Writing – review & editing, Supervision, Funding acquisition.

Author contributions

H.W., Y.D., and **Y.Z.** conceived the idea, discussed the results, and prepared the manuscript. **H.W.** studied the theoretical model of TDE-SWIS. **H.W., X.X.**, and **J.F.** set the experiment and did the electrical measurement. **H.W.** analyzed the experiment result and studied the TDE-SWIS signal coupling methods. **J.L.** helped on the data processing. **H.W.** designed the integrated TDE-SWIS device and finished the demonstrations. **C.C.** helped on the selection and calibration of commercial sensors. **X.X.** and **Z.F.** helped on discussions and preparation of the manuscript. **G.H.** helped revise the manuscript.

Declaration of Competing Interest

The authors declare the following financial interests/personal relationships which may be considered as potential competing interests: A patent based on this research has been submitted. The following manuscript authors are involved in the patent application: Haoyu Wang, Yuan Dai, Yunlong Zi. The other authors declare that they have no competing interest.

Data availability

The data that support the findings of this study are available from the corresponding author upon reasonable request.

Acknowledgement

This work was funded by HKSAR Research Grants Council General Research Fund (Grant no. 14200120), Tencent University Relations Programme (contract no. T-576-INV-20200507-01), and Guangdong Basic and Applied Basic Research Foundation (Project No.: 2020A1515111161). This work was supported in part by the project of Hetao Shenzhen-Hong Kong Science and Technology Innovation Cooperation Zone (HZQB-KCZYB-2020083).

Appendix A. Supporting information

Supplementary data associated with this article can be found in the online version at doi:10.1016/j.nanoen.2022.107982.

References

[1] S.Y. Kim, et al., Sustainable manufacturing of sensors onto soft systems using self-coagulating conductive Pickering emulsions, Sci. Robot. 5 (2020), eaay3604.
[2] A. Al-Fuqaha, M. Guizani, M. Mohammadi, M. Aledhari, M. Ayyash, Internet of things: a survey on enabling technologies, protocols, and applications, IEEE Commun. Surv. Tutor. 17 (2015) 2347–2376.
[3] Su, K., Li, J. & Fu, H. , Smart city and the applications, in: Proceedings of the International Conference on Electronics, Communications and Control (ICECC), 1028–1031 (2011).
[4] J. Li, et al., A tissue-like neurotransmitter sensor for the brain and gut, Nature 606 (2022) 94–101.
[5] M. Bariya, H.Y.Y. Nyein, A. Javey, Wearable sweat sensors, Nat. Electron. 1 (2018) 160–171.
[6] Z. Song, et al., Wireless self-powered high-performance integrated nanostructured-gas-sensor network for future smart homes, ACS Nano 15 (2021) 7659–7667.
[7] M. Majid, et al., Applications of wireless sensor networks and internet of things frameworks in the industry revolution 4.0: a systematic literature review, Sensors 22 (2022) 2087.
[8] W. Gao, et al., Fully integrated wearable sensor arrays for multiplexed in situ perspiration analysis, Nature 529 (2016) 509–514.
[9] H.U. Chung, et al., Binodal, wireless epidermal electronic systems with in-sensor analytics for neonatal intensive care, Science 363 (2019), eaau0780.
[10] H. Wang, J. Wang, X. Xia, D. Guan, Y. Zi, Multifunctional self-powered switch toward delay-characteristic sensors, ACS Appl. Mater. Interfaces 12 (2020) 22873–22880.
[11] J. Wang, H. Wang, K. Yin, Y. Zi, Tribo-induced color tuner toward smart lighting and self-powered wireless sensing, Adv. Sci. 8 (2021), 2004970.
[12] Y. Yang, et al., A laser-engraved wearable sensor for sensitive detection of uric acid and tyrosine in sweat, Nat. Biotechnol. 38 (2020) 217–224.
[13] A. Moin, et al., A wearable biosensing system with in-sensor adaptive machine learning for hand gesture recognition, Nat. Electron. 4 (2021) 54–63.
[14] F. Wen, Z. Zhang, T. He, C. Lee, AI enabled sign language recognition and VR space bidirectional communication using triboelectric smart glove, Nat. Commun. 12 (2021) 5378.
[15] T. Jin, et al., Triboelectric nanogenerator sensors for soft robotics aiming at digital twin applications, Nat. Commun. 11 (2020) 5381.
[16] R.E. Ciez, J.F. Whitacre, Examining different recycling processes for lithium-ion batteries, Nat. Sustain. 2 (2019) 148–156.
[17] X. Hu, L. Xu, X. Lin, M. Pecht, Battery lifetime prognostics, Joule 4 (2020) 310–346.
[18] E.H. Ledet, et al., Implantable sensor technology: from research to clinical practice, J. Am. Acad. Orthop. Surg. 20 (2012) 383–392.
[19] F.-R. Fan, Z.-Q. Tian, Z. Lin Wang, Flexible triboelectric generator, Nano Energy 1 (2012) 328–334.
[20] Z.L. Wang, Entropy theory of distributed energy for internet of things, Nano Energy 58 (2019) 669–672.
[21] L. Wang, et al., System level design of wireless sensor node powered by piezoelectric vibration energy harvesting, Sens. Actuators A Phys. 310 (2020), 112039.
[22] Y.J. Kim, et al., High-performance self-powered wireless sensor node driven by a flexible thermoelectric generator, Energy 162 (2018) 526–533.
[23] H. Wu, et al., Multi-parameter optimized triboelectric nanogenerator based self-powered sensor network for broadband aeolian vibration online-monitoring of transmission lines, Adv. Energy Mater. 12 (2022) 2103654.
[24] K. Dong, Z.L. Wang, Self-charging power textiles integrating energy harvesting triboelectric nanogenerators with energy storage batteries/supercapacitors, J. Semicond. 42 (2021), 101601.
[25] Y. Song, et al., Wireless battery-free wearable sweat sensor powered by human motion, Sci. Adv. 6 (2020), eaay9842.
[26] S. Lu, et al., Simultaneous energy harvesting and signal sensing from a single triboelectric nanogenerator for intelligent self-powered wireless sensing systems, Nano Energy 75 (2020), 104813.
[27] X. Xia, H. Wang, P. Basset, Y. Zhu, Y. Zi, Inductor-free output multiplier for power promotion and management of triboelectric nanogenerators toward self-powered systems, ACS Appl. Mater. Interfaces 12 (2020) 5892–5900.
[28] T. Hu, H. Wang, W. Harmon, D. Bamgboje, Z.L. Wang, Current progress on power management systems for triboelectric nanogenerators, IEEE Trans. Power Electron 37 (2022) 9850–9864.
[29] H. Wang, J. Fu, J. Wang, L. Su, Y. Zi, Tribophotonics: an emerging self-powered wireless solution toward smart city, Nano Energy 97 (2022), 107196.
[30] H. Wang, et al., A paradigm shift fully self-powered long-distance wireless sensing solution enabled by discharge-induced displacement current, Sci. Adv. 7 (2021), eabi6751.
[31] P.F. Wilson, M.T. Ma, Fields radiated by electrostatic discharges, IEEE Trans. Electromagn. Compat. 33 (1991) 10–18.

Haoyu Wang received his B.Eng. degree in Smart Grid Information Engineering from University of Electronic Science and Technology of China in 2018. He joined the Nano Energy and Smart System laboratory in The Chinese University of Hong Kong since February 2019. His research interests mainly focus on mechanical energy harvesting, sensors, and self-powered wireless system.

Dr. Xin Xia received her B.S. degree from Xi'an Jiaotong University in 2018 as a top graduate student. She has joined the Chinese University of Hong Kong as a Ph.D. student since August 2018, as a member of the Nano Energy and Smart System laboratory, and graduated in July 2022. Recently, she is a research associate of Hong Kong University of Science and Technology (Guangzhou). Her current research interests include mechanism of contact electrification and discharge, high-voltage applications of triboelectric nanogenerators, self-powered sensing systems, and novel energy harvesting technologies.

Dr. Jingjing Fu received her Ph.D. degree from the Chinese University of Hong Kong in 2022. Afterwards, she works as s a postdoctoral fellow at the Hong Kong Polytechnic University. Her research interests are mainly focused on the mechanism of triboelectrification, optimizing the energy harvesting system of TENG, tribo-wireless sensor, tribophotonics, the fluid dynamics based on triboelectric effect, and so on. She can be reached by: jingjing.fu@polyu.edu.hk.

Jianan Li received the B.Sc. Degree in Mechatronics Engineering from Northwestern Polytechnical University, in 2019, and the M.Sc. degree in Human and Biological Robotics from Imperial College London, in 2021. He is currently pursuing a PhD degree in Computer Science and Engineering at The Chinese University of Hong Kong. He has worked as an intern at Tencent Robotics X Lab between 2021 and 2022. His research interest is in Artificial Intelligence for Medical Robots.

Chaojie Chen is currently a Ph.D. student in the department of Mechanical and Automation Engineering at the Chinese University of Hong Kong. He received his B.Eng. degree from the Department of Materials Science and Engineering at the University of Science and Technology Beijing in 2018. Then, he received his M.Eng. degree from the Department of Materials Science and Engineering at Tsinghua University in 2021. His research interests are piezoelectric nanogenerator, wearable sensors, and self-powered system.

Dr. Yuan Dai received her B.S. degree from University of Illinois, Urbana- Champaign (UIUC) in 2012, and her Ph.D. degree from University of California, Los Angeles (UCLA) in 2018, both in electrical and computer engineering. Since Jan. 2019, she has been with Tencent, where she is a senior researcher with Robotics X. She has published more than 20 papers in Nature Communications, Science Advances, ACS Nano, Nano Energy, Nano Letters etc., and held 14 patents. Her main research interests include Nano/Microelectromechanical Systems (N/MEMS), sensors, actuators, wearable devices, machine learning, Internet of Things (IoTs), and robotics.

Prof. Zhiyong Fan is a professor at the Department of Electronic and Computer Engineering, HKUST. He obtained his Bachelor and Master degrees from Fudan University, PhD degree from University of California, Irvine. He worked at UC Berkeley as a postdoc (2007–2010). Currently he is a fellow of the Royal Society of Chemistry and a founding member of The Hong Kong Young Academy of Sciences. His interests are in the design and fabrication of novel nanostructures and nanomaterials for high-performance optoelectronics, energy harvesting devices, and sensors.

Prof. Guobiao Hu is a tenure-track assistant professor at the Hong Kong University of Science and Technology (Guangzhou). He obtained his Ph.D. degree in Mechanical Engineering from the University of Auckland, Master and Bachelor degrees from Southwest Jiaotong University. Before joining HKUST-GZ, he worked as a research fellow at Nanyang Technological University for two years. His research interests include vibration energy harvesting, small-scale wind energy harvesting, and acoustic-elastic metamaterials. Dr. Hu has published more than 70 peer-reviewed technical papers in prestigious SCI journals and international conferences. He was a recipient of the Best Paper Finalist Award at the SPIE conference on Smart Structures/NDE in 2018. He serves as reviewer for more than 40 journals and guest editor for several SCI journals, such as the Journal of Physics D: Applied Physics and the ASCE Journal of Environmental Engineering.

Prof. Yunlong Zi joined Hong Kong University of Science and Technology (Guangzhou) as an Associate Professor since July 2022. He was an Assistant Professor in Department of Mechanical and Automation Engineering at the Chinese University of Hong Kong since 2017. Dr. Zi received his Ph.D. in Physics from Purdue University in 2014; his Bachelor of Engineering in Materials Science and Engineering from Tsinghua University in 2009. Before joining CUHK, he worked as a Postdoctoral Fellow at Georgia Institute of Technology during 2014–2017. His current research interests mainly focus on high-efficiency mechanical energy harvesting through triboelectric nanogenerators (TENG), triboelectric effect, discharge, TENG triggered high-voltage applications, and self-powered systems. As the 1st and corresponding authors, his research studies have been published in top-notch journals, including Nature Nanotechnology, Nature Communications, Science Advances, Advanced Materials, Nano Letters, ACS Nano, Nano Energy, and etc. He was honored as Nano Energy Award winner 2021; Fellow of International Association of Advanced Materials (FIAAM) 2021; Vebleo Fellow 2021; MRS Postdoctoral Award winner 2017; Emerging Investigator by Journal of Materials Chemistry C in 2018; MINE Young Investigator Finalist in 2018; and one of "5 students who are transformation makers" as highlighted in Purdue homepage in 2013.